NAVAL POSTGRADUATE SCHOOL
Monterey, California

D D C

RECEIVED
MAY 9 1972
- B -

THESIS

Amplitude Modulation of a Stationary
Acoustic Field by Cavitation Bubbles

by

Walter William Scherf

Thesis Advisor: A. I. Eller

December 1971

Approved for public release; distribution unlimited.

Amplitude Modulation of a Stationary
Acoustic Field by Cavitation Bubbles

by

Walter William Scherf
Lieutenant, United States Navy
B.A., Columbia University, 1963

Submitted in partial fulfillment of the
requirements for the degree of

MASTER OF SCIENCE IN ENGINEERING ACOUSTICS

from the

NAVAL POSTGRADUATE SCHOOL
December 1971

Author _____

Approved by: _____
                                             Thesis Advisor

_____
                                             Reader

_____
          Chairman, Department of Physics

_____
                                     Academic Dean

ABSTRACT

An experimental investigation was made of the modulation of an acoustic standing-wave field due to trapped, cavitation-induced bubbles. Maximum acoustic pressures generated are on the order of 0.1 bar. It is verified that bubbles driven below resonance are trapped just above pressure antinodes of the standing-wave field; bubbles driven above resonance, just above nodes. Maximum modulation percentages of the standing-wave field by bubble scattering are found to be in the neighborhood of up to 12%. Modulation noise spectrum levels are recorded and are found to decrease from 2.5 Hz to 100 Hz with slopes ranging from -3.2 to -5.4 dB/octave. Less than 1% of the modulation noise energy lies in the region above 100 Hz.

TABLE OF CONTENTS

I. INTRODUCTION

This paper concerns the effects of cavitation-induced bubbles in amplitude modulating a medium intensity (from about 0.02 bar (rms) to about 0.15 bar (rms)) standing wave field. The bubbles, after generation, are trapped at the nodes or anti-nodes of an acoustic standing wave field, and at sufficiently high driving levels dance around. Because all of the bubbles generated are grouped fairly closely in size around that value which would be resonant at the exciting field frequency, they act as good sound scatterers. The constant generation, growth in size, dancing about and eventual escape of the trapped bubbles causes the scattered acoustic energy to modulate randomly the exciting carrier signal. The purpose of this research was to measure the frequency spectra for this random modulation signal.

Preliminary to development of these spectra, however, it was necessary to investigate the nature of the standing wave field, which led directly into another interesting and as yet little explored area, namely, the nature of individual bubble motion or dynamics. It was felt that a description (largely qualitative due to equipment and time limitations) of individual and aggregate bubble behavior would be useful, both as an area for study in itself and as providing a possible clue to the nature of the observed sound spectra.

Thus, the investigation resolved itself into three broad areas, namely, the nature of the standing wave field, the development of the scattered noise modulation spectra, and the nature and characteristics of bubble motion within the field.

Although quite a bit of research had been conducted on cavitation bubbles and cavitation noise, the above areas have been relatively unexplored. In some early observations, Boyle (Ref. 1) and Hopwood (Ref. 2) demonstrated that bubbles tend to collect at the pressure nodes of a vertical standing wave pattern. Somewhat later, Blake (Ref. 3) showed that bubbles would also collect at pressure anti-nodal positions, provided that the resonance frequency of the bubble is greater than that of the applied sound field. Eller (Ref. 4) provided a theoretical explanation for the trapping process and calculated the minimum pressure amplitude required to trap a bubble. Strasberg and Benjamin (Ref. 5) observed that if the applied field were strong enough, the trapped bubbles would dance about erratically.

II. THEORY

This section contains a theoretical discussion of the standing wave field and of certain aspects of bubble dynamics. A rigorous treatment of the exceedingly complex modal structure within the tank and of the minute erratic motions of the visible bubbles under the influence of the acoustic field is beyond the scope of this paper. Therefore, the following assumptions are made:

1) The presence of pressure release boundaries at all surfaces. This is true at the water surface, but only approximately so at the sides and bottom of the tank, which are of thin glass.

2) Perfect perpendicularity of the tank sides, and that the water surface is parallel to the tank bottom, neither of which is exactly true.

3) The non-existence of any discrete lines in the spectrum of the noise modulation signal. In fact, none were detected; however, weak frequency components may have been present.

A. THE STANDING WAVE FIELD

The following discussion follows that in Morse (Ref. 6). We consider a rectangular tank measuring 60 cm by 35 cm in length and width respectively, and filled to a depth of 17 cm with water. A rectangular coordinate system is established as in Figure 1 below.
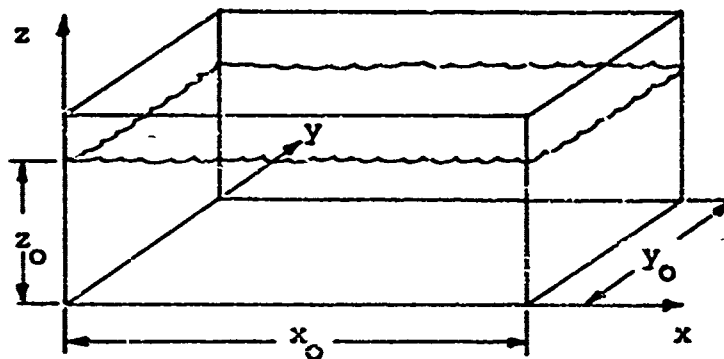
FIGURE 1

The wave equation in rectangular coordinates is

$$\frac{\partial^2 p}{\partial x^2} + \frac{\partial^2 p}{\partial y^2} + \frac{\partial^2 p}{\partial z^2} = \frac{1}{c^2}\frac{\partial^2 p}{\partial t^2} \qquad (1)$$

where x, y, and z are spatial coordinates, and p is acoustic pressure.
Solutions to Equation (1) are of the form

$$p = p_a \sin(\omega_x \frac{x}{c} + \phi_x)\sin(\omega_y \frac{y}{c} + \phi_y)\sin(\omega_z \frac{z}{c} + \phi_z)\exp(-2\pi i f t) \qquad (2)$$

where $f = \frac{1}{2\pi}[\omega_x^2 + \omega_y^2 + \omega_z^2]^{\frac{1}{2}}$ and ϕ_x, ϕ_y and ϕ_z are determined by the

boundary conditions. If we assume that all boundaries are pressure
release, the ϕ's are all zero and we have

$$p = p_a \sin(\omega_x \frac{x}{c})\sin(\omega_y \frac{y}{c})\sin(\omega_z \frac{z}{c})\exp(-2\pi i f t) \qquad (3)$$

where $\omega_x = \frac{c}{x_o}m_x \pi$, $m_y = 1,2,3....$ Similarly, we have $\omega_y = \frac{c}{y_o}m_y \pi$,

$\omega_z = \frac{c}{z_o}m_z \pi$ where m_y, $m_z = 1,2,3....$ The m_x, m_y, m_z are related by

$$f = \frac{\omega c}{4\pi}[(\frac{m_x}{x_o})^2 + (\frac{m_y}{y_o})^2 + (\frac{m_z}{z_o})^2]^{\frac{1}{2}} \qquad (4)$$

Each of these solutions describes a free vibration mode of the enclosure.
Thus the wavelength measured along any axis must at all times be greater

than $\frac{c}{f}$, as can be demonstrated by substituting values for m_x, m_y and m_z,

7

and calculating the equivalent λ_x, λ_y and λ_z. The lowest frequency mode allowed in the tank corresponds to the (111) mode, where the triplet of numbers represent (m_x m_y m_z) respectively. Applying (4), we have the result that this mode corresponds to a frequency of 4.18 KHz. Below this frequency there can exist no standing wave structure in the tank. At discrete frequencies above this cutoff, resonant modes can exist, the frequencies being determined by the triplet (m_x m_y m_z). Thus the first several frequencies above the (111) mode, in ascending order, are those corresponding to the triplets (211), (311), (121), (221), (321), (131), (411), etc.

At higher frequencies, the number of modes that can exist within a given frequency band becomes greater and greater. If we treat the ω_x, ω_y, ω_z as components of a three dimensional vector in frequency space it can be shown that the number of modes dN contained within a frequency band df is given by

$$dN = \frac{4\pi f^2 V}{c^3} \qquad (5)$$

where $V = x_o\, y_o\, z_o$ is the volume of water in the tank, so that for our particular tank of water being ensonified with a 30 KHz sinusoidal signal, we should have dN = 12 for a df of 100 Hz. Thus, within a 0.3% frequency spread around 30 KHz we should have about 12 possible modes of vibration.

The driving transducer forces vibrations in the tank, with the result that all modes of vibration can be excited, but those modes lying closest to the exciting frequency are more strongly excited than those further from it. The relative amount of energy present in any mode depends upon the Q of the system, where Q is defined by

$$Q = \frac{f}{f_2 - f_1} \qquad (6)$$

8

where f is the exciting frequency and

f_1 and f_2 are the lower and upper frequencies, respectively, at which the acoustic pressure amplitude is down by 3 dB. A system such as our tank, with a relatively high Q (Q = 200-500), will have most of the vibrational energy concentrated in only a few of the allowed modes grouped around the exciting frequency. The lower the Q of the system, on the other hand, the more evenly will the energy be distributed over a larger number of allowed modes.

B. BUBBLE DYNAMICS

A bubble located in a standing wave acoustic field will experience a net force from that field. This force is due to spatial pressure variations within the field. If bubble pulsation and acoustic pressure are out of phase, that is, if the bubble grows smaller as acoustic pressure increases, then the bubble will tend to be driven toward a pressure antinode. If the reverse condition holds, with bubble size and acoustic pressure being in phase, the bubble will tend to be driven toward a pressure node. These phenomena may be utilized to trap bubbles at relatively stationary positions in an acoustic standing wave field. It can be shown (Ref. 7) that the minimum acoustic pressure amplitude at an antinode necessary to trap a bubble in a standing wave field in the z direction is given by

$$P_{min}^2 = \frac{2\eta g p_o c}{\pi f} \left[\frac{(1-\xi^2)^2 + d^2}{(1-\xi^2)}\right] \tag{7}$$

where $\xi^2 = \frac{\rho \omega^2 R_o^2}{3\eta p_o}$ and is equal to 1.0 at resonance,

R_o is the equilibrium radius of the bubble,

d is a damping term dependent on the contributions due to heat conduction, sound radiation, and viscosity,

9

η is a number between 1.0 and 1.4, depending on whether the bubble

oscillation process is essentially isothermal or adiabatic,

and p_{min} refers to the pressure amplitude (Zero-to-Peak) at a pressure

antinode of the wave field.

In the above result, we have assumed that the wavelength in the z direction

has its smallest possible value, $\frac{c}{f}$. Then (7) gives us the minimum pres-

sure at an antinode at which a bubble will be trapped in the acoustic field

against the force of buoyancy. Figures 2 and 3 give minimum trapping pres-

sure vs bubble size for some typical frequencies. The significance of these

figures is to fix a rough minimum value of the pressure amplitudes at the

anti-modes in the system during the experiment. At a given frequency, the

acoustic pressure necessary to trap a bubble has minimum values just above

and below resonance, and increases as we move away from resonance in either

direction. Bubbles driven below resonance will be trapped, relative to the

z axis, just above pressure maxima, while bubbles driven above resonance

will be trapped just above pressure nodes.

Regarding the trapping process, it is interesting to note that if a pure

modal state or combination of modal states could exist within the tank, there

could be no trapping at frequencies higher than resonance, since modal posi-

tions within the tank would be vertical and horizontal intersecting planes,

and bubbles, once driven to a vertical plane, would experience no further

vertical acoustic force, and would escape. However, due probably to the

absorbtion of acoustic energy at the walls and various perturbation effects,

such as the presence of the transducers (the driving transducer measured about

3 cm in diameter and 4 cm in length), and non-parallelness of the boundaries,

the theoretically predicted vertical nodal planes were not detected in the

sound field, about which more will be said later. Thus, bubbles could be
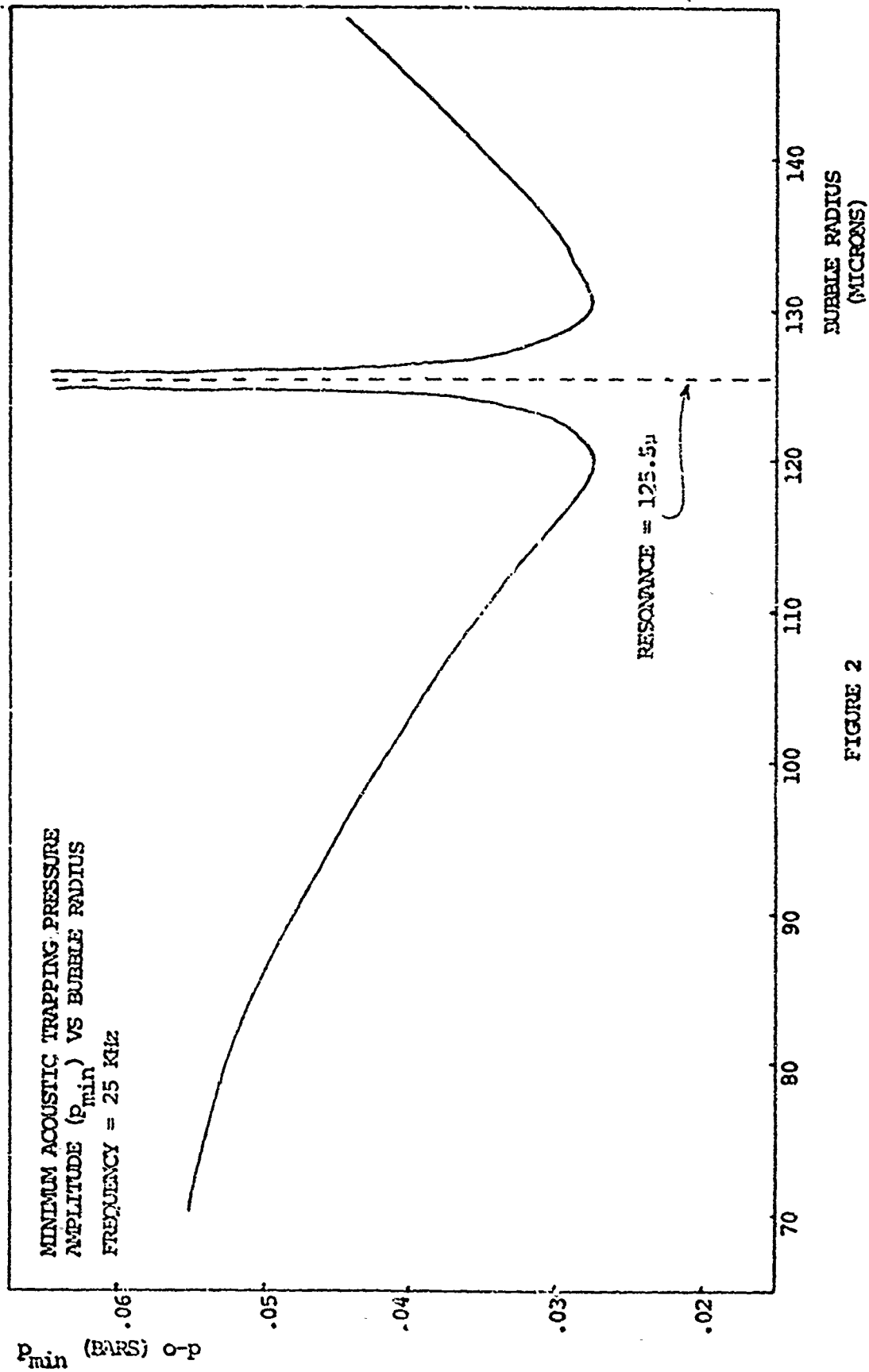
trapped above resonance.

MINIMUM ACOUSTIC TRAPPING PRESSURE
AMPLITUDE (p_{min}) VS BUBBLE RADIUS

FREQUENCY = 25 KHz

RESONANCE = 125.5µ

BUBBLE RADIUS
(MICRONS)

P_{min} (BARS) o-p

FIGURE 2

11

MINIMUM ACOUSTIC TRAPPING PRESSURE
AMPLITUDE (p_{min}) VS BUBBLE RADIUS

FREQUENCY = 30 KHz

RESONANCE = 114u
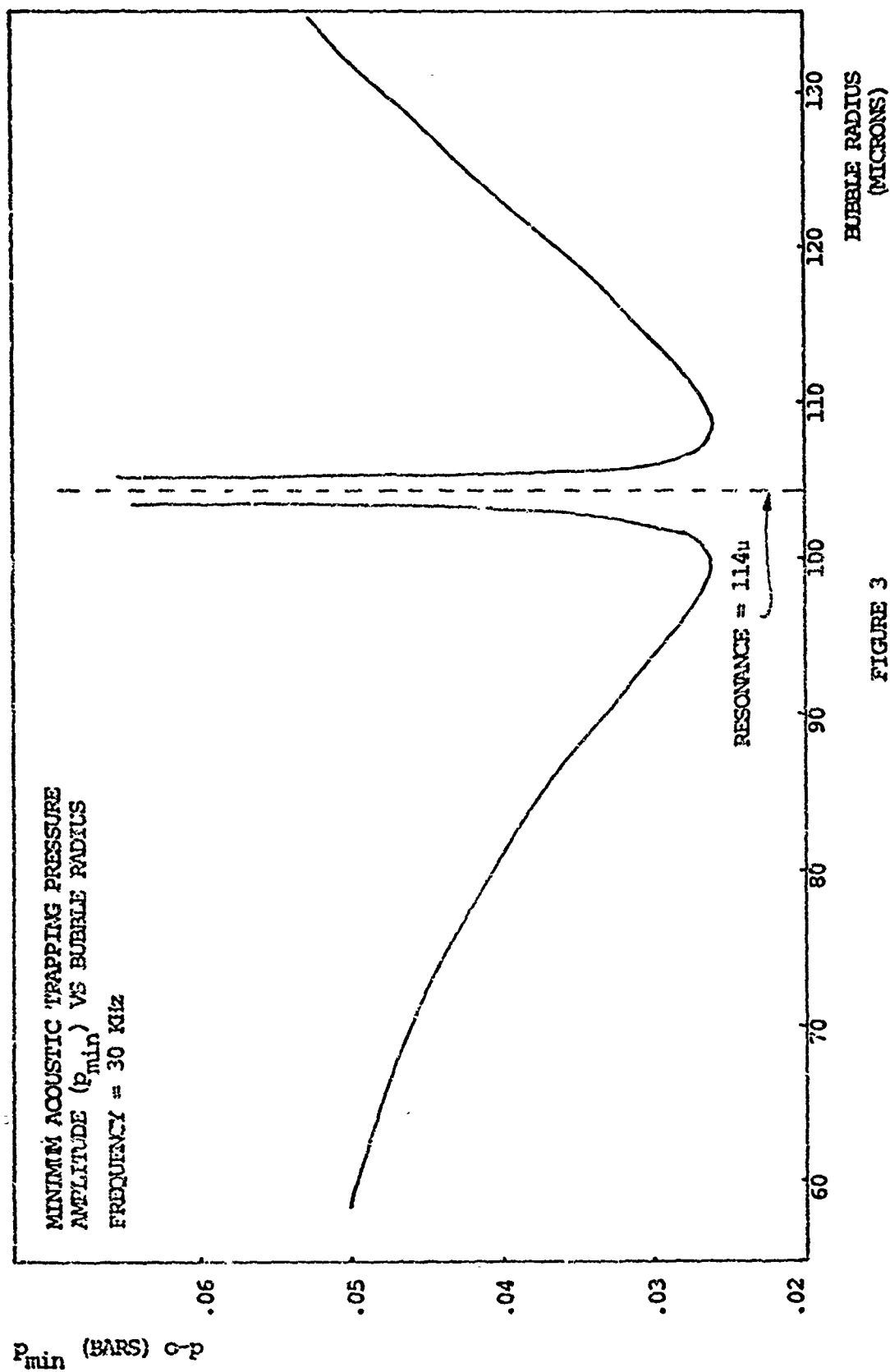
BUBBLE RADIUS
(MICRONS)

p_{min} (BARS) o-p

FIGURE 3

12

III. EXPERIMENTAL PROCEDURE

The arrangement of equipment was completely straightforward and is
illustrated in Figure 4. The sine wave from the signal generator was
amplified and used to drive a PZT-4 transducer. A variable inductor was
connected in series to balance the capacitance of the transducer and
provide a more effective impedance match with that of the amplifier.

The acoustic signal was received on a small 1/8" diameter cylindrical
probe hydrophone, given 40 dB of amplification, passed through a 60 Hz
filter, then either viewed directly or passed through a rectifier and
detector and fed to a 1/3-octave frequency analyzer. Late in the experi-
ment it was discovered that a significant amount of the carrier was being
leaked through the detector, so an additional low-pass filter, a Kronh-Heit
active type, was installed after the detector.

The transducers were installed in a standard 15 gallon fishtank,
measuring 60 x 35 x 30 cm in length, width, and height respectively, and
filled to a depth of 17 cm with water. The driver was clamped permanently
in one corner of the tank and not touched through the experiment, while
the receiving transducer was mounted on a sliding carriage that permitted
it to cover most of the tank, at least horizontally, with facility.

A. MEASUREMENT OF NOISE

The receiving hydrophone was calibrated at the start of the experiment
by direct comparison with a calibrated laboratory standard. All pressure
amplitudes calculated during the course of the experiment were figured
directly from the results of this calibration. At the close of the experi-
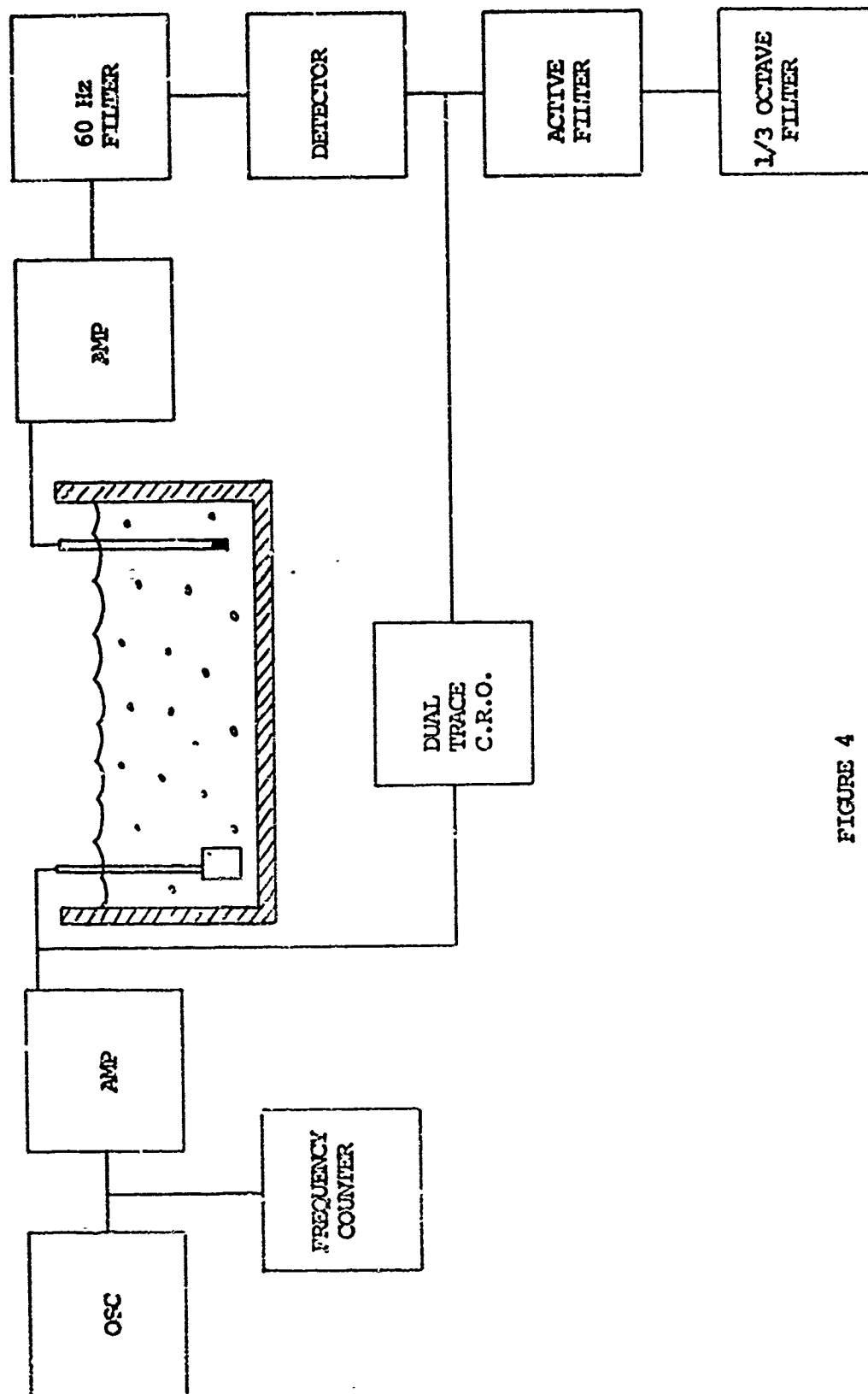ment, the receiving hydrophone was recalibrated. The results of the two

13

FIGURE 4

14

calibrations were within 20%. In general, the pressure measurements contain the largest percentage errors of any of the quantities calculated during the experiment. Their accuracy (pressure amplitude measurements) is estimated at ± 20%.

A typical unfiltered signal, taken directly from the hydrophone (after 40 dB of amplification) is illustrated in Figure 5. Our main interest lay not in the carrier but rather in the irregular amplitude modulation of the carrier.

After the removal of any 60 Hz component present, the signal was passed through a detector, basically a low-pass filter and rectifier, with a -3 dB point of about 1200 Hz. What remains is the amplitude modulation signal as pictured in Figure 6.

Very little could be conjectured about the frequency spectrum of the amplitude modulation signal before it was analyzed, so it was fed into a GR 119 wave analyzer, an instrument with a practical low frequency cutoff of about 20 Hz. It was soon apparent that by far the greatest percentage of the energy in the noise signal lay below that frequency. Therefore, the GR 119 was replaced with a GR 1564 octave band analyzer, which has a low-frequency cutoff of 2.5 Hz, and the noise measurements were made on that. As opposed to the GR 119, which had a constant width gate (3,10 or 50 Hz), the GR 1564 was capable of operating in a 1/10 or 1/3 octave mode; the latter mode was used in the experiment. However, the GR 119 was used during several runs (using the 3 Hz gate) to search for discrete components in the noise signal.

The 1/3 octave band level readings obtained were corrected to spectrum level using the conversion:

SPECTRUM LEVEL (dB) = BAND LEVEL (dB) - 10 log Δf

15
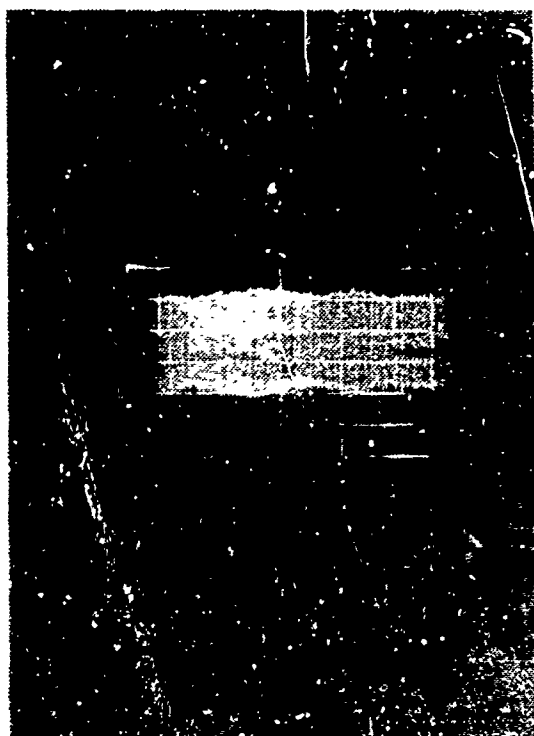
AMPLITUDE MODULATED
CARRIER SIGNAL

CARRIER FREQ = 29.751 KHz

DRIVING LEVEL CORRESPONDS TO
HIGHEST USED (70V RMS)

VERTICAL SENSITIVITY:
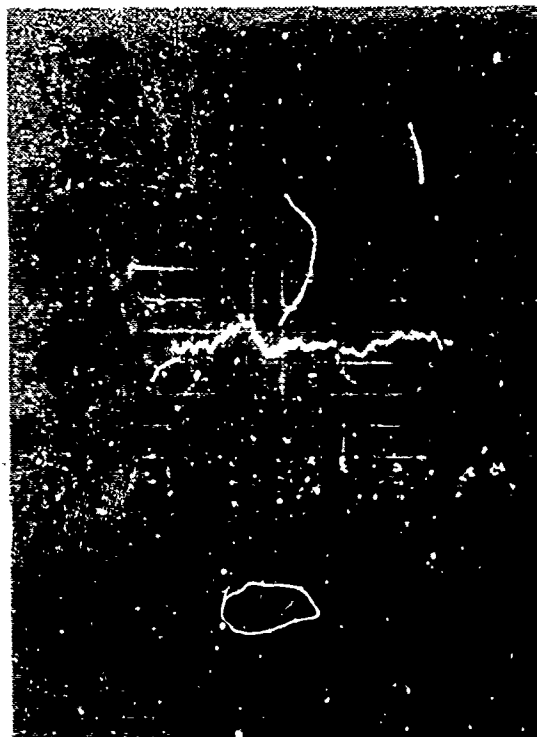1 VOLT/CM

HORIZONTAL SWEEP:
0.2 SEC/CM

FIGURE 5

RECTIFIED AND FILTERED
CARRIER SIGNAL

CARRIER FREQUENCY
AND DRIVING LEVEL
SAME AS ABOVE

VERTICAL SENSITIVITY:
0.2 VOLT/CM

HORIZONTAL SWEEP:
0.2 SEC/CM

FIGURE 6

16

where Δf is the frequency spread of the band in question. Spectrum level is then the average amount of energy per hertz bandwidth that one measures in any band. The GR handbook has a table of Δf values for the 1/3 octave band used in the experiment.

B. OBSERVATION OF BUBBLE MOTION

The original experiment was not set up for the purpose of investigating bubble dynamics within the tank, and the apparatus and general setup did not lend themselves to the taking of precise, quantitative data in this area. However, the bubble dynamics proved so interesting in itself that it was decided to include a section describing, qualitatively, bubble effects, and some rough calculations of bubble size as related to trapping pressures.

The bubble generation and trapping process was observed through the tank, side illuminated against a black backcloth. This system provided excellent contrast and good viewing.

A bubble's size was determined from its velocity of ascent through the water by using Stokes' Law. The assumption was made that the bubbles' shapes remained spherical as they rose, and no attempt was made to apply empirical corrections to Stokes' Law calculations, since these corrections were small compared to the error in determining the bubble's position and its time of rise. The procedure used was to let the bubble field stabilize for a few minutes, then to select a bubble, and by holding a ruler externally against the tank, determine its vertical position. Parallax errors were reduced to as small a value as possible by eyeball. The sound field was then rapidly shut off; a stopwatch being started at the same time. The bubble's time of ascent to the surface was then determined, the velocity thereby calculated, and Stokes' Law, in the following form, employed to find bubble radius:

17

$$P^2 = (\frac{9\nu}{2g})\mu \qquad\qquad (8)$$

where ν, the kinematic viscosity, = 0.0093 poise, appropriate for 23°C

g = 980 cm/sec

μ = bubble velocity

R = bubble radius in cm

A plot of R vs μ is given in Figure 7 below.

STOKES' LAW PREDICTION OF
BUBBLE SIZE VS VELOCITY
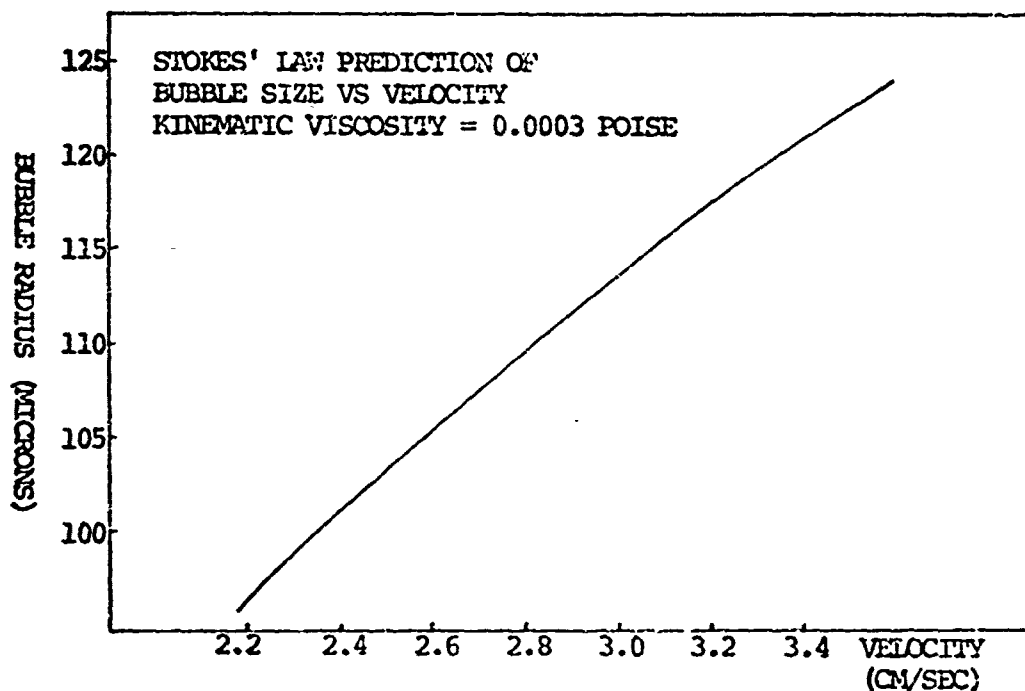KINEMATIC VISCOSITY = 0.0003 POISE

FIGURE 7

C. CALCULATION OF Q

Typical values for Q were calculated by tuning the frequency generator to get a relative peak in the carrier signal, then fine tuning it to locate the -3 dB points. This procedure is valid only as long as a single mode is present over the range of frequencies in question; that is, from the lower

18

3 dB point to the higher 3 dB point. Typical values for this frequency spread ranged from 50 Hz to 250 Hz. Refer to Table 1. Our previous calculations, however, indicate that at 30 KHz, we should expect about 12 vibrational modes per 100 Hz bandspread. In actuality, although some modes were extremely close together, too close to permit a calculation Q, there were numerous modes, which, to the eye, appeared to be the only significant mode present over a bandspread of several hundred hertz, and thus permitted calculating values for Q. It is not understood why so many fo the theoretically possible model configurations are absent, or at least, unmeasurable.

D. MEASUREMENT OF MODULATION PERCENTAGE

Modulation percentage, as defined here, is the ratio of the rms filtered modulation signal to the rms modulated carrier. The rms filtered modulation voltage was measured on the GR-1564 octave band analyzer, using the all-pass band. During measurements of modulation percentage, the hydrophone was located at a position in the sound field where the carrier was a relative maximum.

E. MEASUREMENT OF PRESSURE AMPLITUDE

The receiving hydrophone was calibrated by comparison with a laboratory standard. The receiving signal, regardless of further process ', was given 40 dB of amplification. The actual receiving hydrophone sensitivity was 0.01 volt (rms) = 0.016 bar (rms). However, all scales on the graphs included herein represent actual meter readings, that is, with the addition of 40 dB amplification. Therefore, we have that 1.0 volt (rms) = 0.016 bar (rms).

19

IV. EXPERIMENTAL RESULTS

A. ACOUSTIC WAVE FIELD

The sound field, in spatial configuration, when probed along a line parallel to one of the boundaries at frequencies above the low-frequency cutoff, demonstrated the expected sinusoidal pattern. At relatively low frequencies the mode shape came close to agreeing wit'1 the theoretical description of a pure mode. At higher frequencies however, the mode shape appeared to be the sum of several modes of oscillation. Typical field patterns are shown in Figure 8 and 9. These patterns were made at low driving levels so that the effect of modulation noise was minimal. The expected sinusoidal shape is evident, although the differing heights of the various peaks indicate the presence of more than one mode in the tank. Note also that at no node does the acoustic pressure amplitude go to zero, indicating that the walls of the tank are not true non-absorptive pressure release boundaries.

An attempt was made to construct the (111) mode within the tank, without success. The lowest obtainable modal configuration was the (311) mode, at a measured 5.3 KHz.

It is difficult to give representative values of Q. As the frequency generator was swept over a range of frequencies from, say, 10KHz through 40 KHz, with the receiving hydrophone placed at an arbitrary spot in the tank, there were observed hundreds of stronger and weaker resonances. Many of these resonances were so close to each other that the separation between them was less than the frequency spread necessary to measure the -3 dB points. Several resonances at various frequencies are tabulated in

TRANSVERSE SPATIAL CARRIER
VOLTAGE VARIATION
FREQUENCY = 31.722 KHz
1.0 VOLT (RMS) = 0.016 BAR (RMS)

VOLTS (RMS)

0.4

0.3

0.2

0.1

MEASURED
REGION

Y_O

Z_O

0   5   10   15   20   25

CENTIMETERS

FIGURE 9

LONGITUDINAL SPATIAL CARRIER
VOLTAGE VARIATION
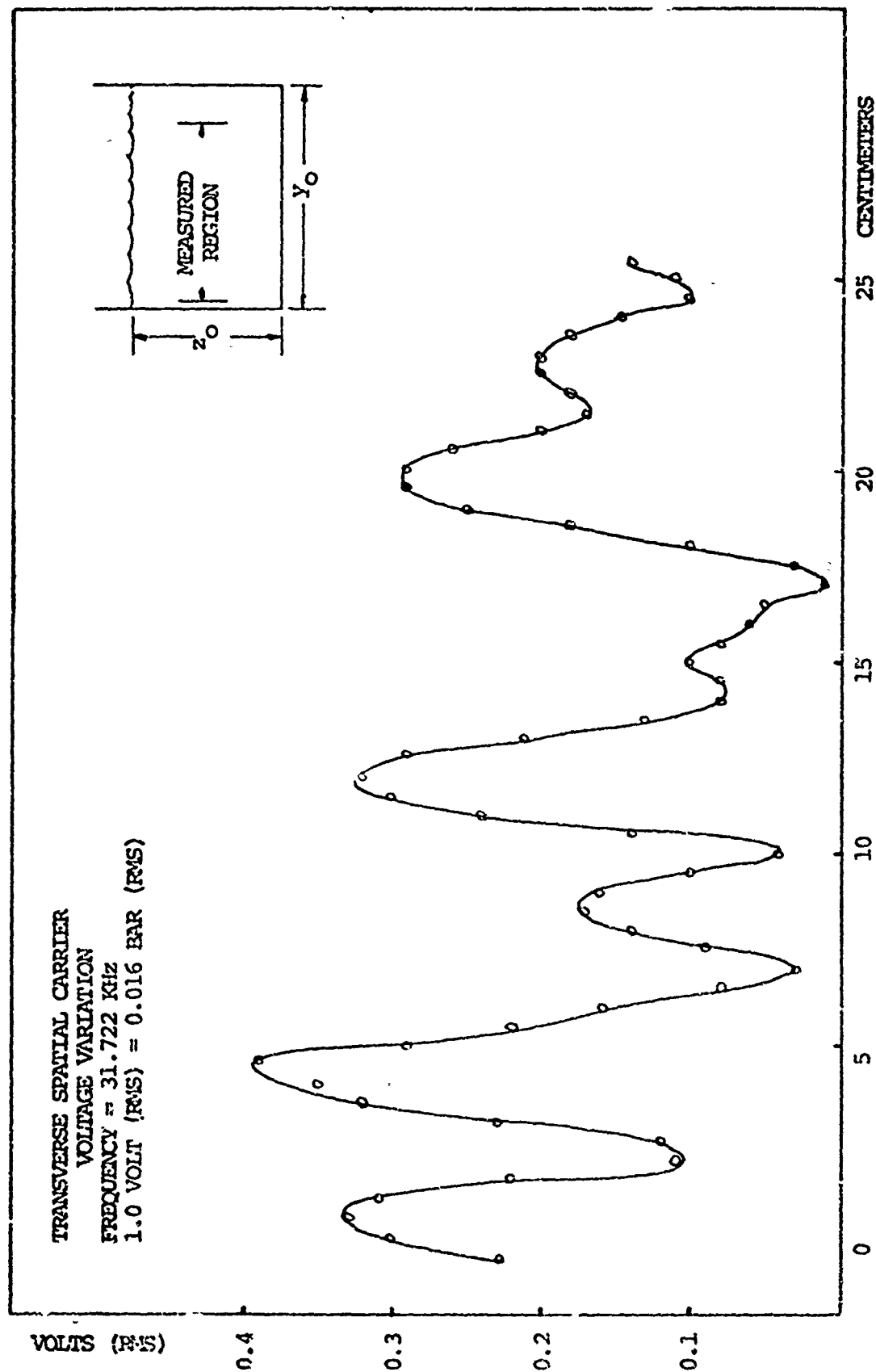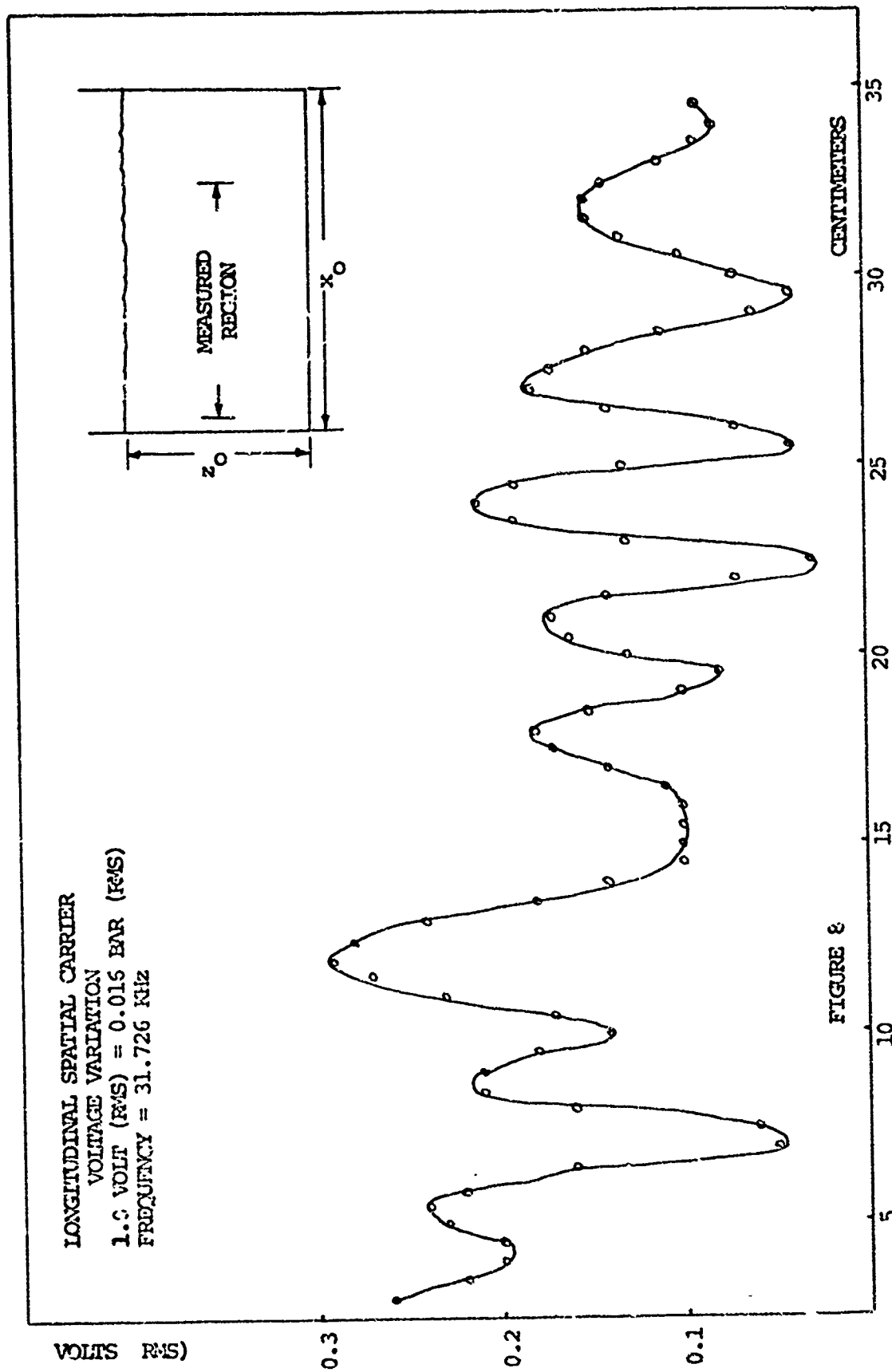**1.5 VOLT (RMS)** = 0.015 BAR (RMS)
FREQUENCY = 31.726 KHz

FIGURE 8

22

Table 1 below. The three values at each frequency correspond to different positions in the tank. For a given mode, then, the values for Q do not differ by more than about 20%.

TABLE 1: Representative Values of Q

Frequency (KHz)	Δf	Q
25.711	54	474
	69	372
	60	429
27.050	120	226
	105	258
	136	198
30.207	163	197
	170	178
	191	158
31.271	130	240
	132	254
	144	218
32.543	102	319
	115	282
	121	269

In the theoretical calculations it was determined that there should exist about 12 possible modes within a 100 Hz band centered at 30 KHz. In fact, only two or three are observable. Changing the positions of the sending or receiving hydrophones did not increase the number of observed modes at a given frequency.

B. MODULATION SPECTRUM

Figure 6 shows a typical output signal, taken directly from the receiving hydrophone, and given 40 dB amplification. Here V_{in} = 70 volts (rms) which corresponds to the maximum driving levels used during the experiment. Cavitation was severe and the bubble field was stabilized.
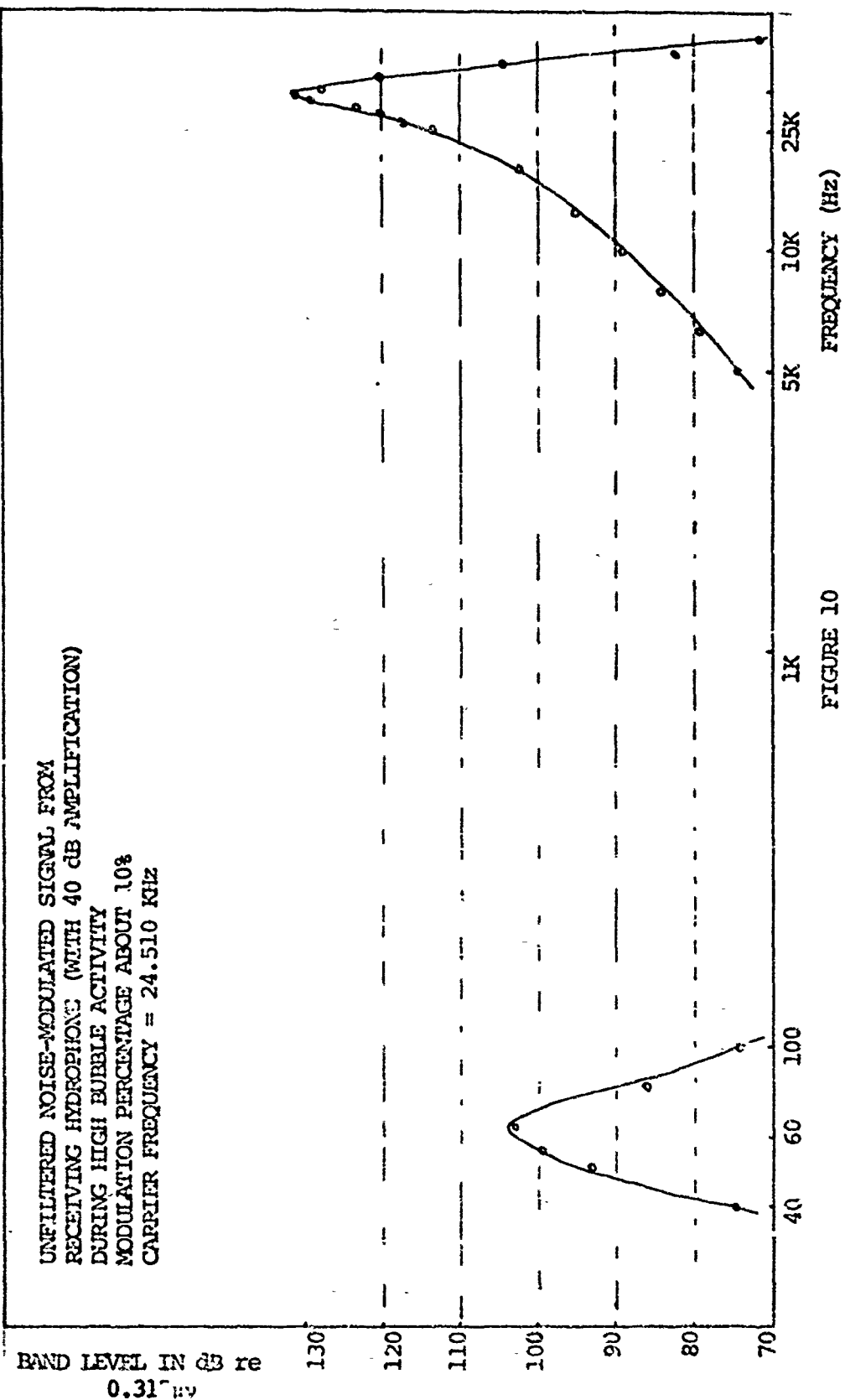
23

UNFILTERED NOISE-MODULATED SIGNAL FROM
RECEIVING HYDROPHONE (WITH 40 dB AMPLIFICATION)
DURING HIGH BUBBLE ACTIVITY
MODULATION PERCENTAGE ABOUT 10%
CARRIER FREQUENCY = 24.510 KHz

FIGURE 10

BAND LEVEL IN dB re 0.317 μv

FREQUENCY (Hz)

The low frequency modulation is apparent. Figure 10 shows a representative unfiltered carrier frequency spectrum, with 40 dB of amplification. Here we are also driving at a high level, and the modulation percentage is about 10%. The lower hump in Figure 10 is a measure of the 60 Hz noise interference in the output signal from the amplifier, while the upper hump is the carrier signal and its noise modulation products on either side.

Measurements of the modulation percentage indicate that at the maximum driving levels used, the modulation percentage was on the order of 8-12%. The filtered modulation signal corresponding to the unfiltered signal in Figure 6 is shown in Figure 7. The vertical sensitivity of the CRO has been increased to better delineate the signal. Reference to the horizontal sweep time rate indicated that a large amount of the signal's energy lies at very low frequencies (less than 10 Hz).

Typical noise modulation spectra are shown in Figures 11, 12, and 13. As can be seen, the spectrum level in every case diminishes in magnitude from the lower to the higher frequencies. In no case did the amount of energy in the modulation spectrum above 80 Hz amount to as much as 1% of the total energy in the rectified signal. One apparent discrepancy evident in Figures 11, 12, and 13 is the fact that the total energy of any signal measured was 2-3 dB greater than the sum of the individual bands added together. The only explanation offered is that this could be an idiosyncrasy of the GR 1564 or might be a consistent error in data recording, namely, a constant lower-than-actual reading of the dB meter. This could amount to a considerable error in the summation of 17 bands, which was the number used. During measurement of these modulation spectra,

SPECTRUM LEVEL VS MODULATION FREQUENCY
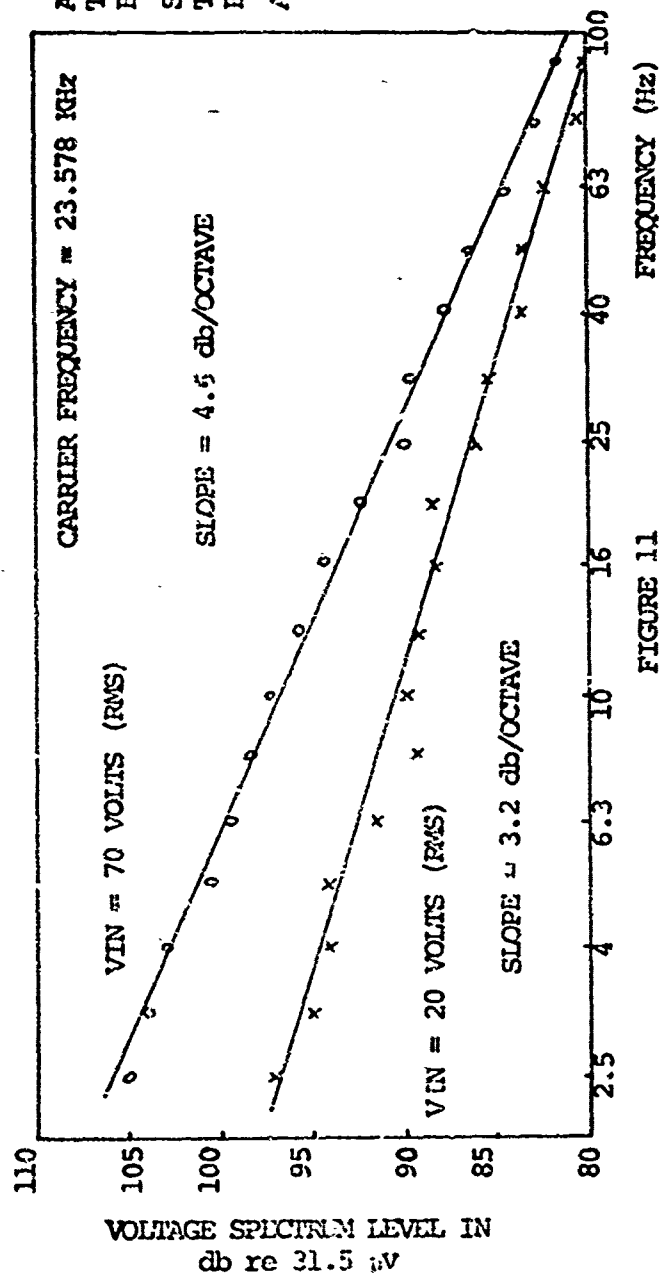AT DIFFERENT DRIVING LEVELS

CARRIER FREQUENCY = 23.578 KHz

ALL PASS BAND:
TOP: 113 db
BOTTOM: 106 db

SUM OF INDIVIDUAL BANDS:
TOP: 110.7 db
BOTTOM: 103.2 db

ALL db re 0.315μν

SLOPE = 4.5 db/OCTAVE

VIN = 70 VOLTS (RMS)

VIN = 20 VOLTS (RMS)

SLOPE = 3.2 db/OCTAVE

VOLTAGE SPECTRUM LEVEL IN
db re 31.5 μV

FREQUENCY (Hz)

FIGURE 11

26

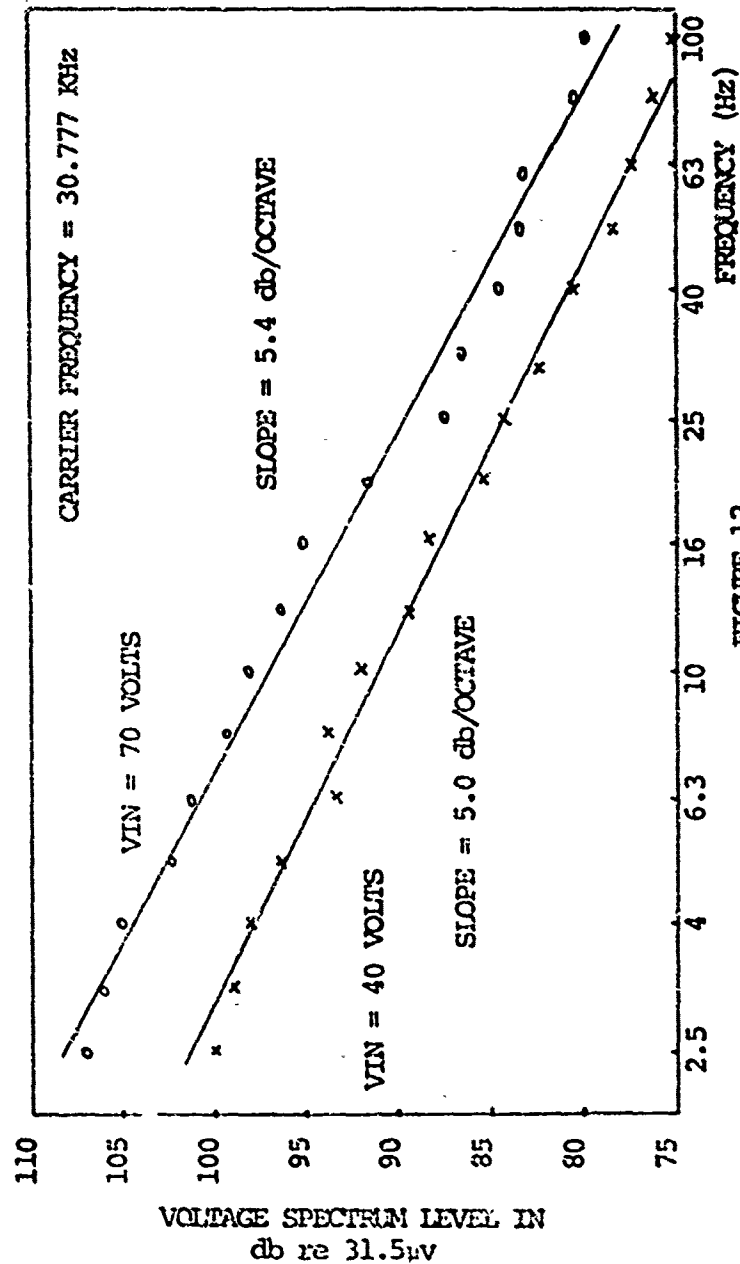SPECTRUM LEVEL VS MODULATION FREQUENCY
AT DIFFERENT DRIVING LEVELS

CARRIER FREQUENCY = 30.777 KHz

ALL PASS BAND:
TOP: 115 db
BOTTOM: 109 db

SUM OF INDIVIDUAL BANDS:
TOP: 112.4 db
BOTTOM: 105.7 db
ALL db re 0.315μv

SLOPE = 5.4 db/OCTAVE
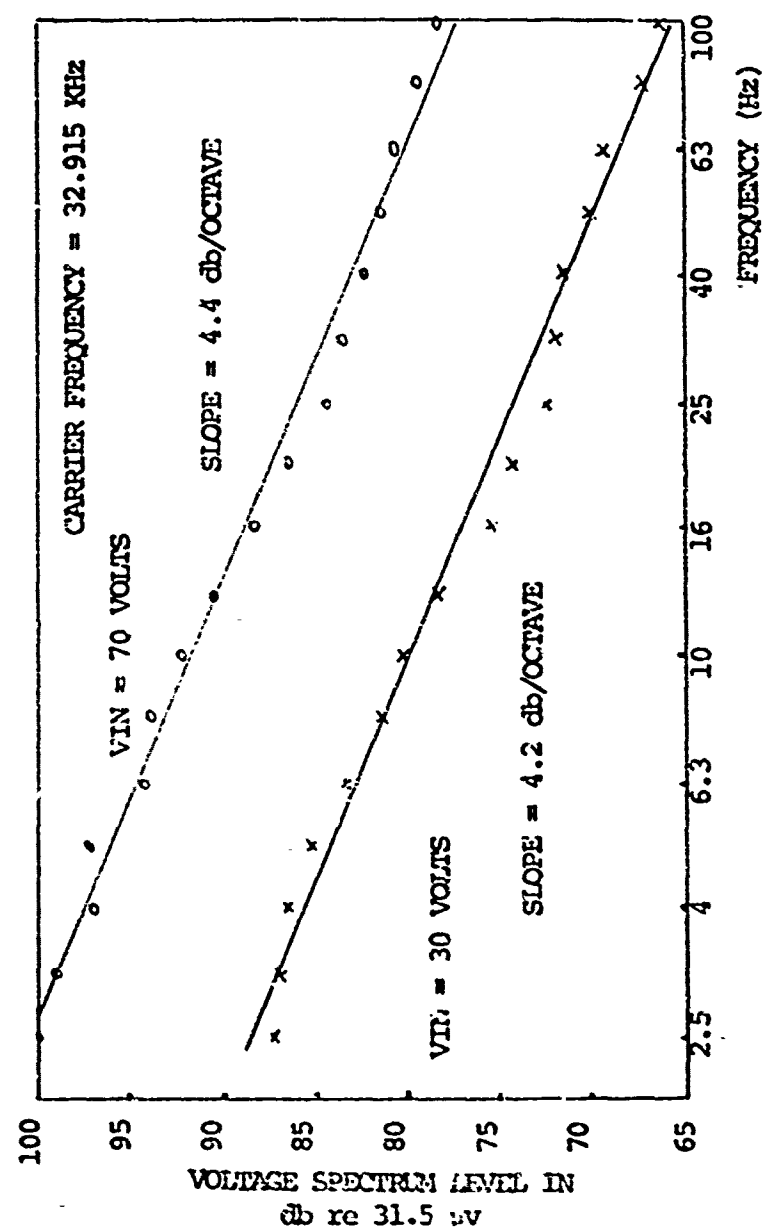
VIN = 70 VOLTS

VIN = 40 VOLTS

SLOPE = 5.0 db/OCTAVE

VOLTAGE SPECTRUM LEVEL IN
db re 31.5μv

FREQUENCY (Hz)

FIGURE 12

SPECTRUM LEVEL VS MODULATION FREQUENCY
AT DIFFERENT DRIVING LEVELS

FIGURE 13

the maximum carrier rms pressure amplitudes were typically in the order of up to 0.04 bars. The percentage modulation was typically from 4% to 12% at positions of maximum carrier amplitude.

C. BUBBLE DYNAMICS

As mentioned earlier, bubble trapping occurs at positions just above either vertical nodes or antinodes, depending on whether the bubble resonance frequency is lower or higher than the accustic exciting field frequency. The lowest frequency at which trapping occured was 5.8 KHz. At this frequency, the vertical pressure amplitude profile consisted of nodes at the surface and bottom of the tank and an antinode in the middle. Thus, only bubbles below resonance were trapped (just above an antinode). At sufficiently high driving levels, the bubbles began to grow (by rectified diffusion) and finally escaped to the surface. The time from trapping to final escape, at this frequency, was on the order of 15-30 seconds at the highest driving levels used.

At the driving frequencies used for most of the study, that is, above about 25 KHz, the vertical pressure pattern was no longer a single half-wave, but several half-waves, thus permitting nodal as well as anti-nodal trapping. In fact, the higher the driving frequency, the shorter the time time period a given bubble would stay small enough to be trapped in an anti-nodal position. At frequencies above 30 KHz, the time period between observed bubble generation (due to cavitation) and the jump from an anti-nodal to a nodal trapped position was not more than several tenths of a second and could not be quantitatively measured with the available equipment. Bubbles trap above their resonance frequency (that is, at nodal positions), were generally stable, and depending on the driving voltage amplitude, would maintain their positions for several minutes at a time.

29

The number of trapped bubbles in the tank at a given time was dependent upon the driving frequency, driving voltage amplitude, and the length of time the field had been activated. At an estimate, the number varied between 15 and 50 bubbles. Generally, there seemed to be no preferred nodal or antinodal positions, and the trapping process occured fairly uniformly throughout the tank. Quantitatively, the all-pass noise modulation signal was measured for several different frequencies and driving levels, as a function of receiving probe position. Under no combination of driving frequency and amplitude did the variation within the tank exceed 2 dB.

Given a trapped bubble at a fixed frequency, the increase in its motion at higher driving levels was quite marked. At lower levels, the trapped bubbles were almost stationary, merely undergoing small excursions about an equilibrium position. As the driving voltage was increased, the motion became more violent, following an ellipsoidal path. At the highest driving levels obtainable, the bubble motion amounted to excursions of as much as a centimeter (estimated by eye). At these levels, the acoustic pressure amplitude amounted to on the order of 0.15 bar (rms).

D. MEASURED BUBBLE SIZES

Bubble sizes calculated through application of Stokes' Law revealed that the smallest measured, trapped bubble had a radius of 85 microns, in an exciting field of 30.744 KHz. Resonance size at this frequency was 104 microns. Thus, at a given frequency, there was a large variation in bubble size on each side of resonance.

V. CONCLUSIONS

1. Bubbles trapped in a stationary acoustic field cause scattering of acoustic energy and can amplitude modulate the ensonifying acoustic field.

2. Bubbles can be trapped below and above resonance, near anti-nodes and nodes of the standing wave field, respectively.

3. Carrier signal pressure amplitudes of about 0.07 bar (rms) produced severe bubble motion.

4. At pressure amplitudes ranging up to about .04 bar (rms), the amplitude modulation percentage was about 8-12% when bubbles were present.

5. For the frequencies and pressures observed, the modulation spectra levels due to the scattered noise decreased with increasing frequency, with slopes that ranged from 3.2 dB to 5.4 dB per octave, over a range of frequencies from 2.5 Hz to 100 Hz.

REFERENCES

1. Boyle, R. W., "Ultrasonic Stationary Waves", Nature 120, 476-477, (1928).

2. Hopwood, F. L., "Ultrasonics: Some Properties of Inaudible Sound", Nature 128, 748-751 (1931).

3. Blake, R. G., "Bjerknes Forces in Stationary Sound Fields", J. Acoust. Soc. Am. 21, 551 (1949).

4. Eller, A. I., "Force on a Bubble in a Standing Acoustic Wave", J. Acoust. Soc. Am. 43, 170-171 (1968).

5. Strasberg, M. and Benjamin, T. B., "Excitation of Oscillations in the Shape of Pulsating Gas Bubbles, Experimental Work", J. Acoust. Soc. Am. 30, 697 (1958).

6. Morse, P. M., Vibration and Sound, 381-429, McGraw-Hill, 1948.

7. Crum, L. A. and Eller, A. I., "The Motions of Bubbles in a Stationary Sound Field", Acoust. Res. Lab. Tech Mem. No. 61, Harvard Univ., 1969.

DOCUMENT CONTROL DATA - R & D

(Security classification of title, body of abstract and indexing annotation must be entered when the overall report is classified)

1. ORIGINATING ACTIVITY (Corporate author)	2a. REPORT SECURITY CLASSIFICATION
Naval Postgraduate School Monterey, California 93940	Unclassified
	2b. GROUP

3. REPORT TITLE

Amplitude Modulation of a Stationary Acoustic Field by Cavitation Bubbles

4. DESCRIPTIVE NOTES (Type of report and inclusive dates)

Master's Thesis; December 1971

5. AUTHOR(S) (First name, middle initial, last name)

Walter William Scherf

6. REPORT DATE	7a. TOTAL NO. OF PAGES	7b. NO. OF REFS
December 1971	35	7

8a. CONTRACT OR GRANT NO.	9a. ORIGINATOR'S REPORT NUMBER(S)
b. PROJECT NO.	
c.	9b. OTHER REPORT NO(S) (Any other numbers that may be assigned this report)
d.	

10. DISTRIBUTION STATEMENT

Approved for public release; distribution unlimited.

11. SUPPLEMENTARY NOTES	12. SPONSORING MILITARY ACTIVITY
	Naval Postgraduate School Monterey, California 93940

13. ABSTRACT

An experimental investigation was made of the modulation of an acoustic standing-wave field due to trapped, cavitation-induced bubbles. Maximum acoustics pressures generated are on the order of 0.1 bar. It is verified that bubbles driven below resonance are trapped just above pressure antinodes of the standing-wave field; bubbles driven above resonance, just above nodes. Maximum modulation percentages of the standing-wave field by bubble scattering are found to be in the neighborhood of up to 12%. Modulation noise spectrum levels are recorded and are found to decrease from 2.5 Hz to 100 Hz with slopes ranging from -3.2 to -5.4 dB/octave. Less than 1% of the modulation noise energy lies in the region above 100 Hz.

DD FORM 1473 (PAGE 1)

S/N 0101-807-6811

A-31408

KEY WORDS	LINK A		LINK B		LINK C	
	ROLE	WT	ROLE	WT	ROLE	WT
Modulation						
Cavitation						
Standing Wave						
Bubbles						